3 Results – Effect of Heat Treatment on Fatigue Life

3.1 Fatigue ε–N Behavior

Several fatigue tests have been completed on two heats of Type 304 SS under various heat–treatment conditions, and in air and simulated BWR and PWR environments at 289°C. The results from these tests and data obtained earlier on MA Heat 30956 are given in Table 2.

Table 2. Fatigue test results for Type 304 stainless steel in air and simulated BWR and PWR environments at 289°C

Test No.	Spec. No.	Environment[a]	Dis. Oxygen[b] (ppb)	pH at RT[c]	Conductivity[b] (μS/cm)	ECP Pt[b] mV (SHE)	ECP SS[b] mV (SHE)	Ten. Rate (%/s)	Comp. Rate (%/s)	Stress Amp. (MPa)	Strain Amp. (%)	Life N_{25} (Cycles)
Heat 30956 MA												
1805	309-03	Air	–	–	–	–	–	4.0E-3	4.0E-1	234.0	0.38	14,410
1853	309-22	BWR	880	6.0	0.06	248	155	4.0E-3	4.0E-1	233.3	0.38	12,300
1856	309-24	BWR	870	6.2	0.07	272	163	4.0E-3	4.0E-1	236.8	0.38	10,450
1808	309-06	PWR	4	6.4	18.87	-693	-690	4.0E-3	4.0E-1	234.2	0.39	2,850
1821	309-09	PWR	2	6.5	22.22	-700	-697	4.0E-3	4.0E-1	237.2	0.38	2,420
1859	309-28	PWR	2	6.5	18.69	-699	-696	4.0E-3	4.0E-1	235.9	0.38	2,420
Heat 30956 MA plus 0.67 h at 700°C												
1893	309-43	Air	–	–	–	–	–	4.0E-3	4.0E-1	236.9	0.38	17,000
1894	309-44	BWR	800	6.7	0.07	263	158	4.0E-3	4.0E-1	239.1	0.38	3,920
1899	309-46	BWR	800	6.2	0.06	285	126	4.0E-3	4.0E-1	241.4	0.38	3,740
1898	309-45	PWR	6	6.3	17.24	-677	-467	4.0E-3	4.0E-1	241.2	0.38	2,530
Heat 30956 MA plus 24 h at 700°C												
1891	309-47	Air	–	–	–	–	–	4.0E-3	4.0E-1	235.8	0.38	16,680
1892	309-48	BWR	860	–	0.06	257	119	4.0E-3	4.0E-1	237.3	0.39	2,790
1897	309-50	PWR	6	6.3	16.67	-629	-543	4.0E-3	4.0E-1	234.1	0.39	2,380
Heat 10285 MA plus 24 h at 600°C												
1895	102-07	Air	–	–	–	–	–	4.0E-3	4.0E-1	222.4	0.38	19,300
1896	102-09	BWR	800	–	0.1	265	206	4.0E-3	4.0E-1	222.2	0.39	1,665
1900	102-08	PWR	7	6.2	16.95	-522	-527	4.0E-3	4.0E-1	228.0	0.37	2,840

[a]PWR = simulated PWR water with 2 ppm Li, 1000 ppm B, and ≈2 ppm dissolved H_2 (or ≈23 cc/kg) in the feedwater; BWR = high-purity deionized water.
[b]Measured in effluent.
[c]RT = room temperature.

The effect of heat treatment on the fatigue life of Type 304 SS in air, BWR, and PWR environments is shown in Fig. 5. Fatigue life is plotted as a function of the EPR value for the various material conditions. The results indicate that heat treatment has little or no effect on the fatigue life of Type 304 SS in air and PWR environments. In a BWR environment, fatigue life is lower for the sensitized SSs. The decrease in life seems to increase with increasing EPR value.

The cyclic stress response of the various materials in air, BWR, and PWR environments at 289°C is shown in Fig. 6. As expected, the cyclic strain–hardening behavior of Type 304 SS under various heat treatment conditions is identical, only the fatigue life varies in the environments.

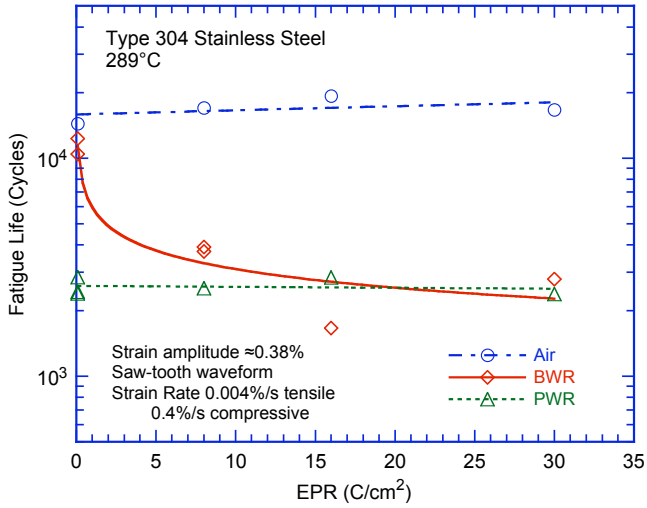

Figure 5.
The effect of material heat treatment on fatigue life of Type 304 stainless steel in air, BWR, and PWR environments at 289°C, ≈0.38% strain amplitude, sawtooth waveform, and 0.004%/s tensile strain rate.

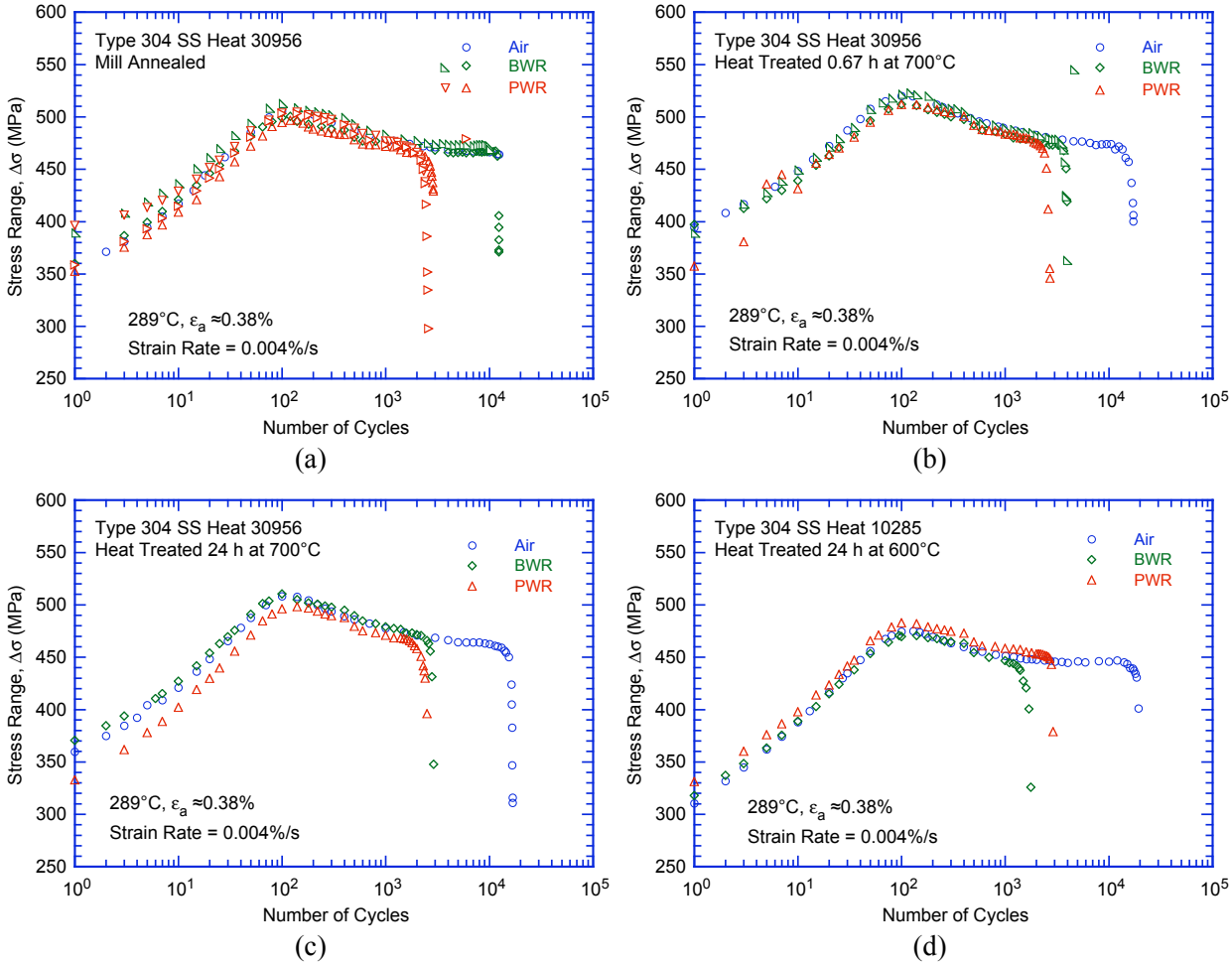

Figure 6. Cyclic stress response of Heat 30956, (a) MA, (b) MA + 0.67 h at 700°C, and (c) MA + 24 h at 700°C; and Heat 10285, (d) MA + 24 h at 600°C, in air, BWR, and PWR environments at 289°C.

3.2 Fatigue Crack and Fracture Surface Morphology

A detailed metallographic evaluation of the fatigue test specimens was performed to characterize the crack and fracture morphology of the various heats under various heat treatment conditions. Figure 7 shows low– and high–magnification crack initiation sites on the fracture surfaces of the sensitized Type 304 SS tested in air. It can be observed that, apparently irrespective of the degree of sensitization, the fracture mode for crack initiation (i.e., crack lengths up to ≈200 μm) and crack propagation (i.e., crack lengths >200 μm) is transgranular (TG), most likely along crystallographic planes, leaving behind relatively smooth facets. With increasing degree of sensitization, cleavage–like or stepped TG fracture (e.g., Figs. 7c and d), and occasionally ridge structures on the smooth surfaces (e.g., Figs. 7e and f) were observed.

An effect of a simulated normal–water chemistry BWR environment, Fig. 8, was to cause intergranular (IG) crack initiation, implying a weakening of the grain boundaries. In the BWR environment, the initial crack appeared IG under all heat–treated conditions. Photomicrographs of the fracture surface of the more heavily sensitized steel, e.g., Heat 30956 MA + 24 h at 700°C (Figs. 8g and h) and especially Heat 10285 MA + 24 h at 600°C (Figs. 8e and f), are good examples of smooth IG fracture. Furthermore, by comparing the four material conditions, it appears that the extent of IG fracture increases with the degree of sensitization, at least through the MA + 24 h at 600°C condition, whereas MA + 24 h at 700°C appears to have a somewhat more mixed IG and TG morphology. Also, one effect of the BWR environment (Figs. 8a–h) was to cause IG crack initiation, implying a weakening of the grain boundaries. Nevertheless, for all four conditions tested, initial IG mode transformed within <200 μm into a TG mode with cleavage–like features. By contrast, for all samples of Type 304 SS tested in PWR environments (Fig. 9), cracks initiated and propagated in a TG mode irrespective of the degree of sensitization. Prominent features of all fracture surfaces are highly angular, cleavage–like fracture facets that exhibit well–defined "river" patterns. Intergranular facets were rarely observed, mostly in the more heavily sensitized alloys. These observations suggest brittle behavior throughout the testing period.

Fatigue striations normal to the crack advance direction were clearly visible beyond ≈200 μm on the fracture surfaces of all materials under all environmental conditions, as documented in Figs. 10–13. For example, for the MA Heat 30956 samples tested in BWR water (Fig. 10), striations were easily discernible on the facets irrespective of the steps, cleavage–like features, or river patterns. Similar striations were also observed on the fracture surface of MA Heat 30956 heat–treated 0.67 h at 700°C irrespective of the testing environment (Fig. 11). Striations were found on both the TG and IG facets of the samples tested under BWR conditions, or co-existing with the "river" patterns specific to the samples tested in the PWR environment. Evidence of extensive rubbing due to repeated contact between the two mating surfaces (Figs. 11a and b) was also found.

Figure 12 shows fatigue striations observed on the fracture surface of MA Heat 10285 heat–treated 24 h at 600°C. In spite of the wide coverage with rubbing and fretting marks, striations are clearly observed on some facets. Figures 12e and f show striations on one IG facet in a sample tested in PWR conditions. The fracture surfaces of MA Heat 30956 heat–treated 24 h at 700°C are presented in Fig. 13. Low– and high–magnification photomicrographs are presented of fatigue striations on faceted, stepped TG, and cleavage–like fracture surfaces.

Air Environment

Heat 30956 mill annealed plus heat treated 0.67 h at 700°C

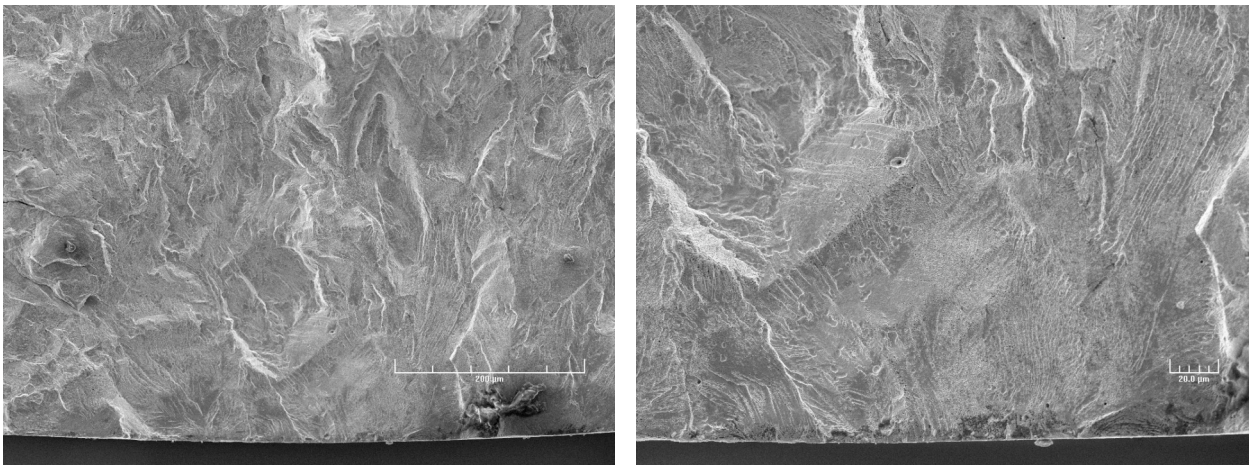

(a) (b)

Heat 10285 mill annealed plus heat treated 24 h at 600°C

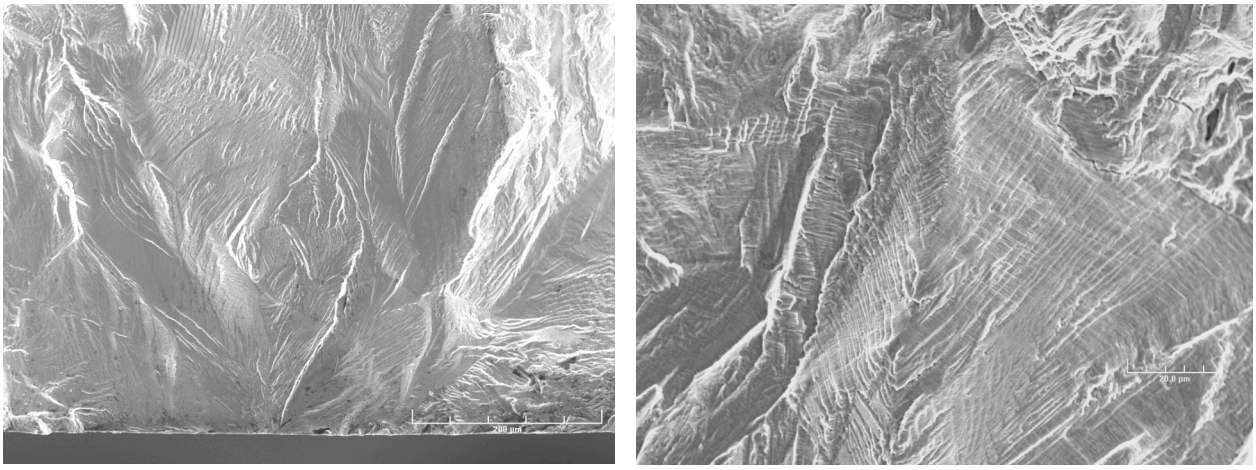

(c) (d)

Heat 30956 mill annealed plus heat treated 24 h at 700°C

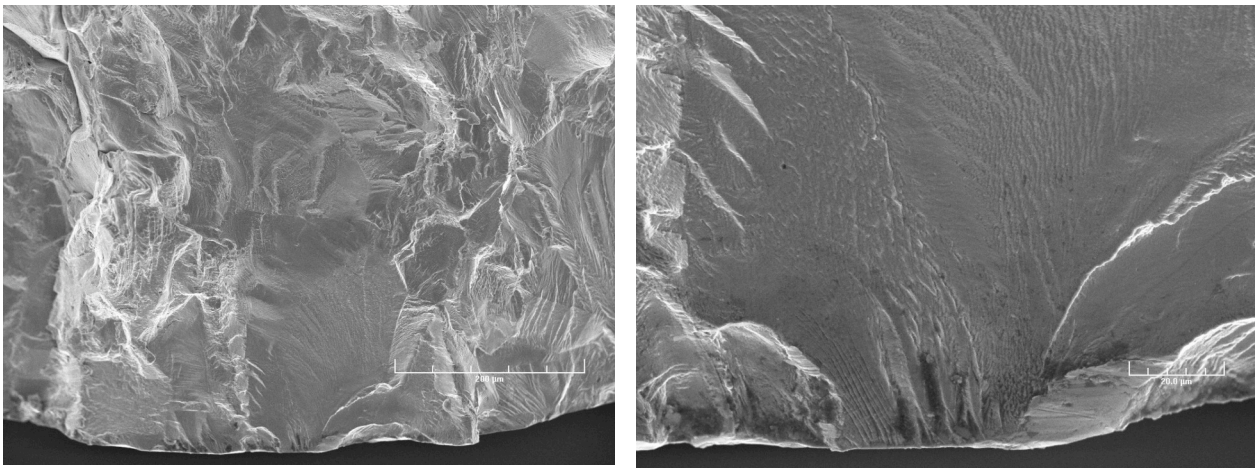

(e) (f)

Figure 7. Photomicrographs showing sites of crack initiation on fracture surfaces of Type 304 SS specimens tested in air: (a), (c), (e), low magnification; (b), (d), (f), high magnification.

Simulated BWR Environment

Heat 30956 mill annealed

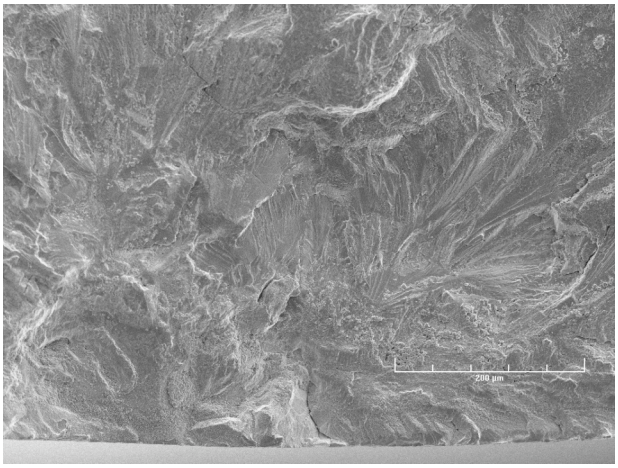

(a)

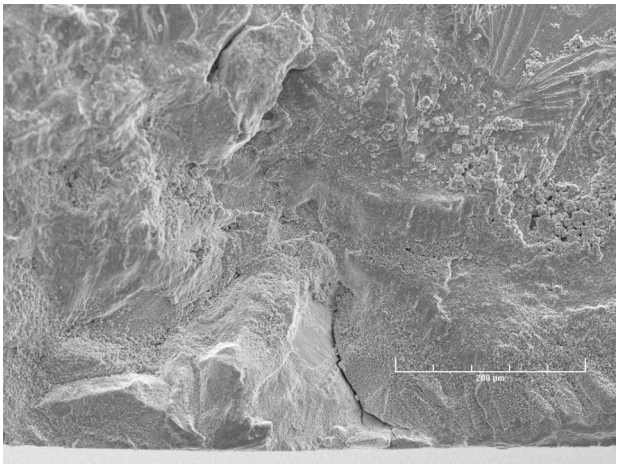

(b)

Heat 30956 mill annealed plus heat treated 0.67 h at 700°C

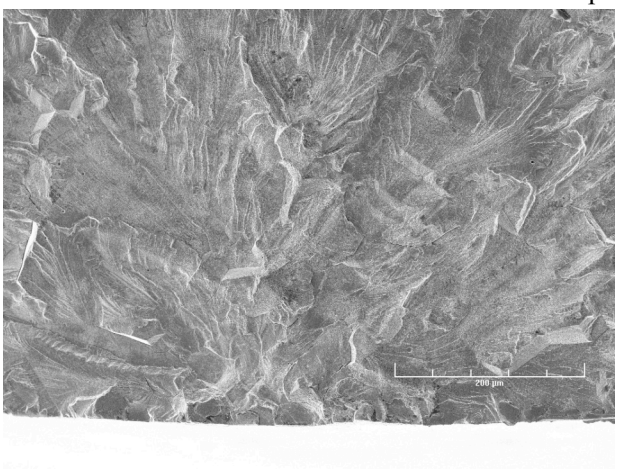

(c)

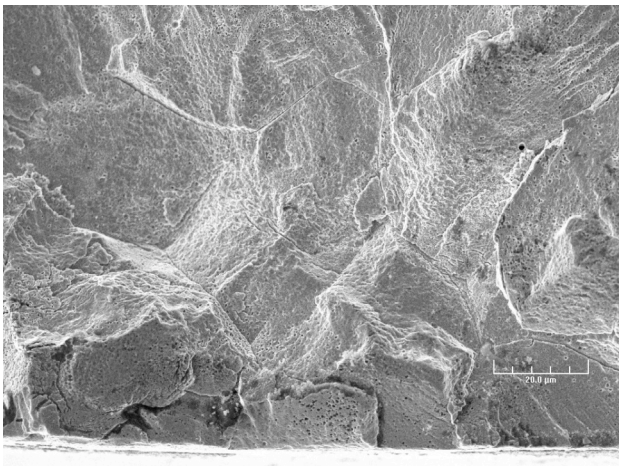

(d)

Heat 10285 mill annealed plus heat treated 24 h at 600°C

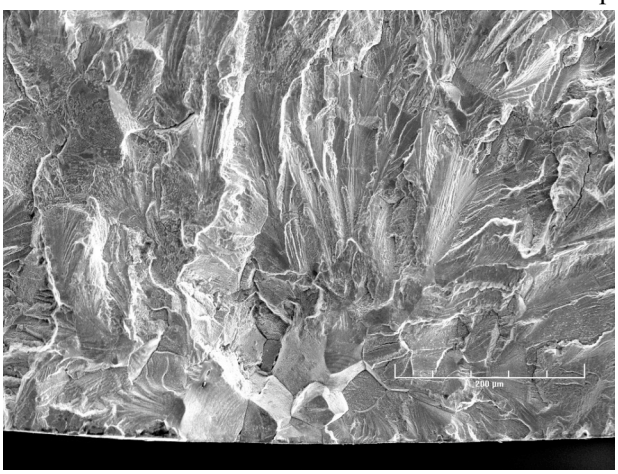

(e)

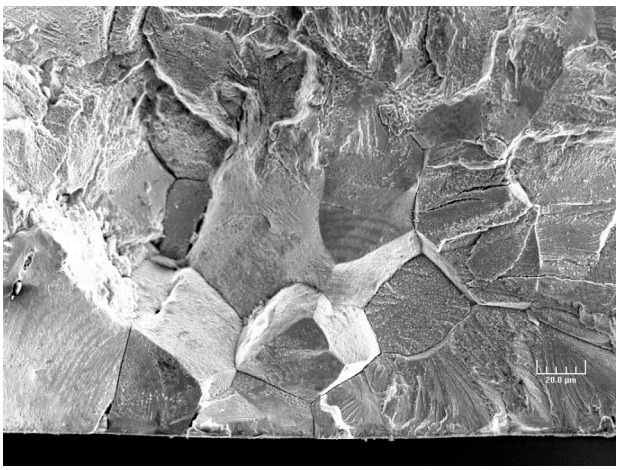

(f)

Heat 30956 mill annealed plus heat treated 24 h at 700°C

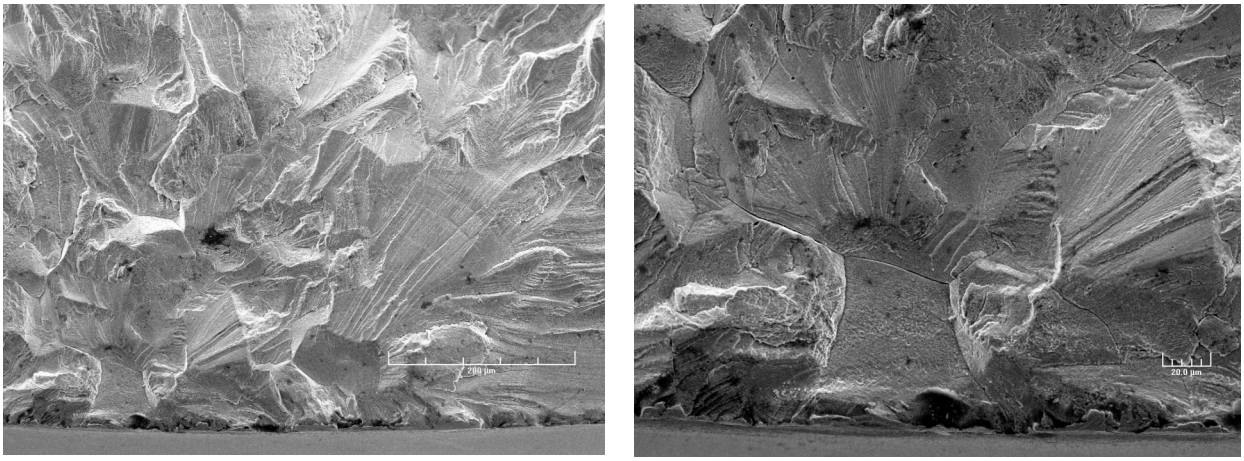

(g) (h)

Figure 8. Photomicrographs showing sites of crack initiation on fracture surfaces of Type 304 SS specimens tested in simulated BWR environment: (a), (c), (e), (g) low magnification; (b), (d), (f), (h) high magnification.

Simulated PWR Environment

Heat 30956 mill annealed

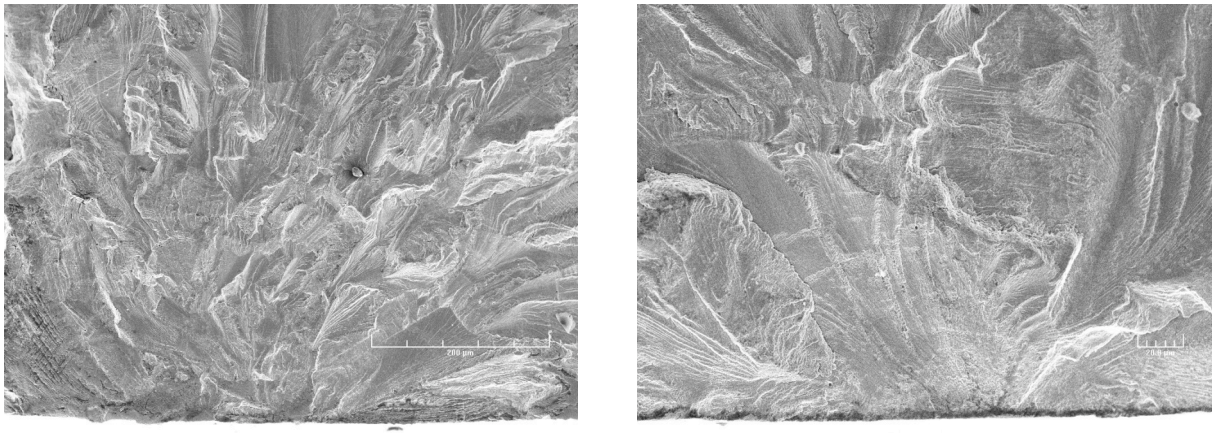

(a) (b)

Heat 30956 mill annealed plus 0.67 h at 700°C

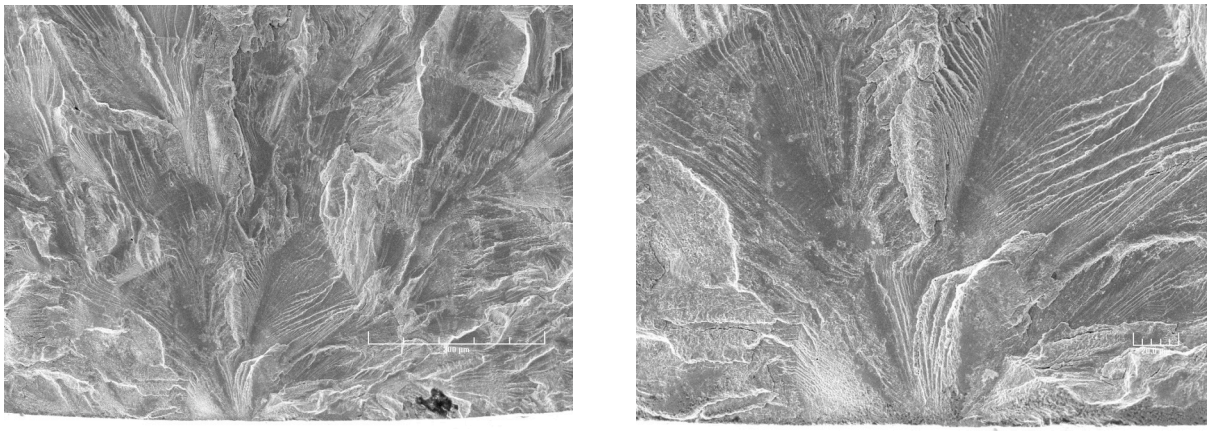

(c) (d)

Heat 10285 mill annealed plus 24 h at 600°C

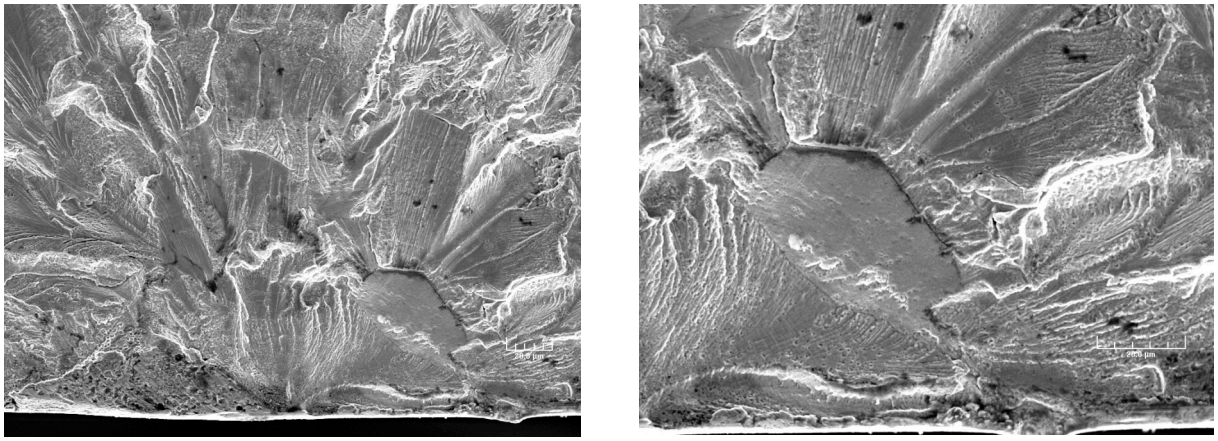

(e) (f)

Heat 30956 mill annealed plus 24 h at 700°C

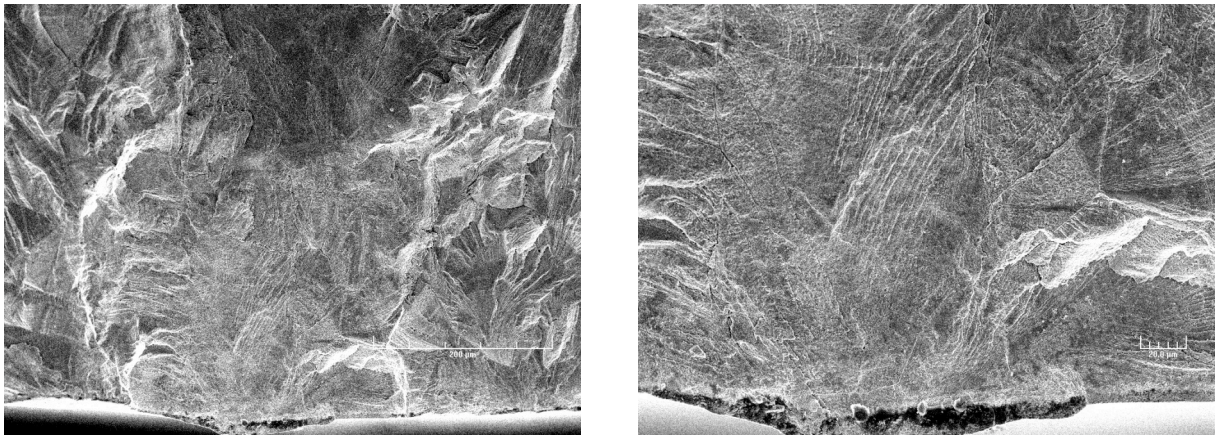

(g) (h)

Figure 9. Photomicrographs showing the sites of crack initiation on the fracture surfaces of Type 304 SS specimen tested in simulated PWR environment: (a), (c), (e), (g) low magnification; (b), (d), (f), (h) high magnification.

Simulated BWR environment

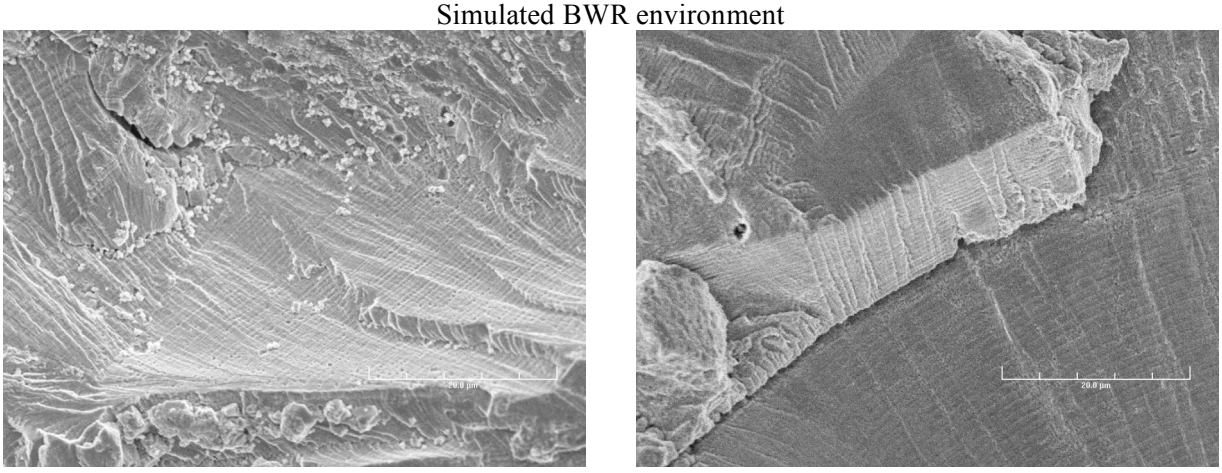

(a) (b)

Figure 10. (a) Low– and (b) high–magnification photomicrographs showing striations at select locations on fracture surfaces of MA specimen of Heat 30956 in simulated BWR environment.

Heat 30956 mill annealed plus 0.67 h at 700°C

Air Environment

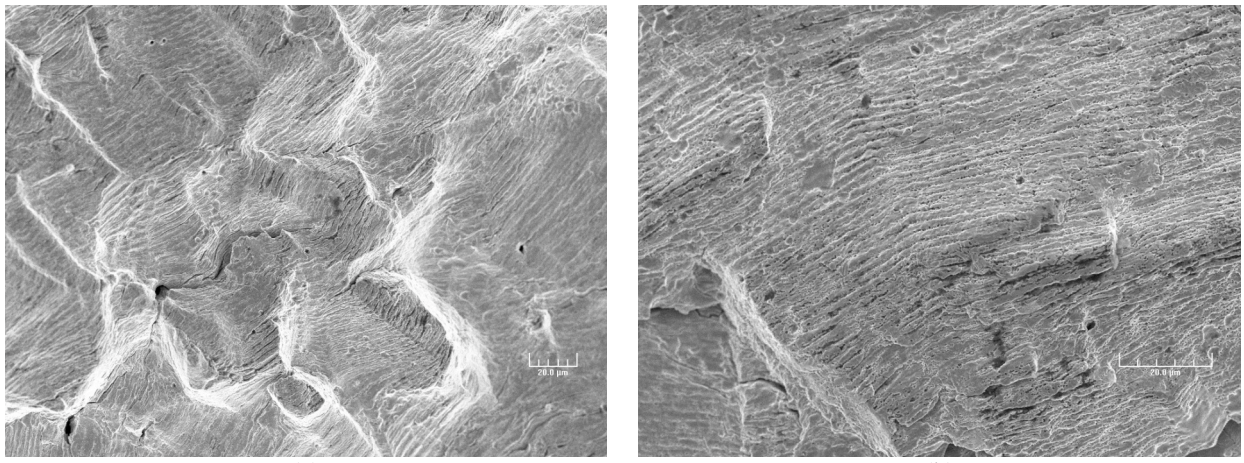

(a) (b)

Simulated BWR Environment

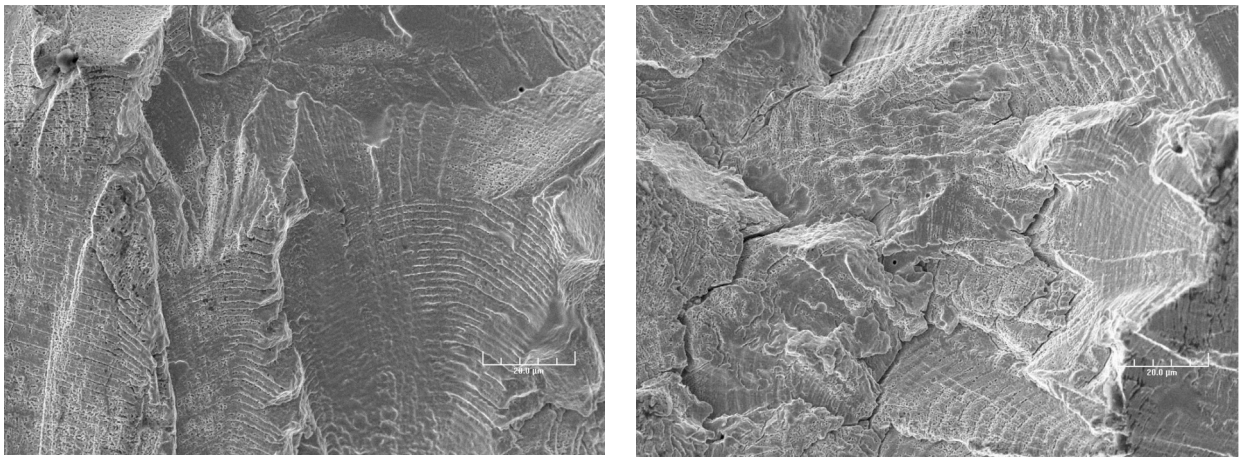

(c) (d)

Simulated PWR Environment

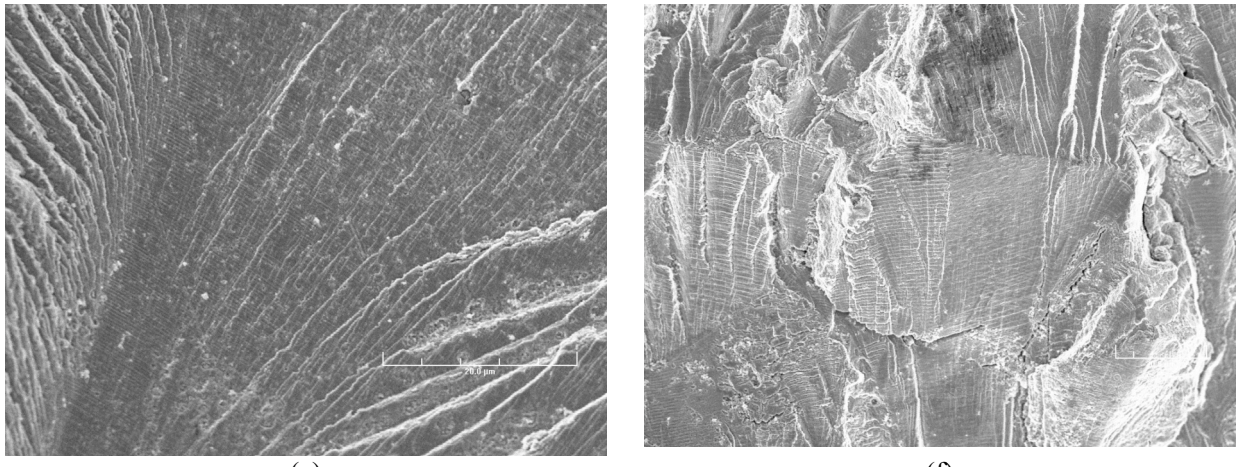

(e) (f)

Figure 11. Low– (a), (c), (e) and high–magnification (b), (d), (f) photomicrographs showing striations at select locations on fracture surfaces of MA specimens of Heat 30956 heat–treated for 0.67 h at 700°C in air, BWR, and PWR environments.

Heat 10285 mill annealed plus 24 h at 600° C

Air Environment

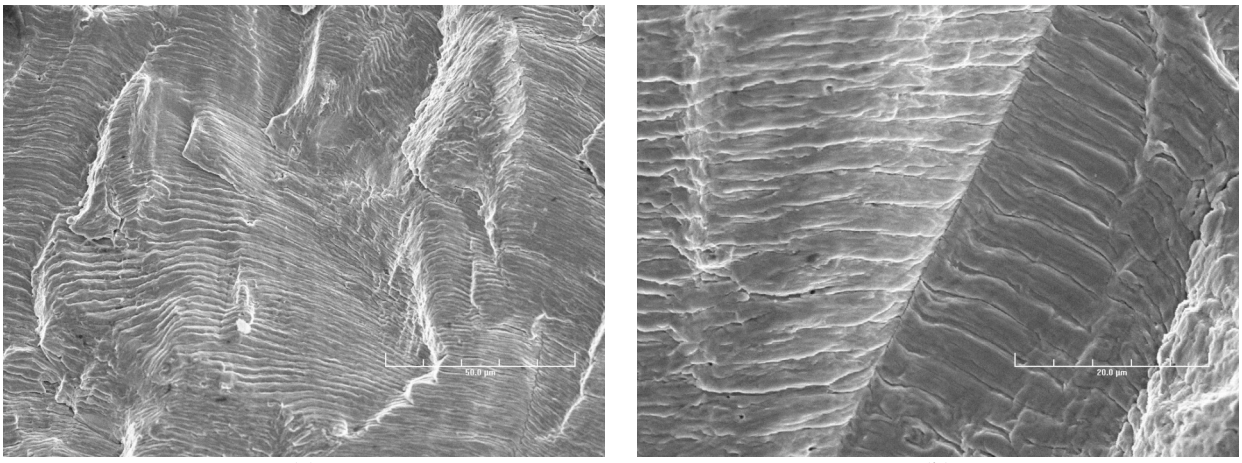

(a) (b)

Simulated BWR Environment

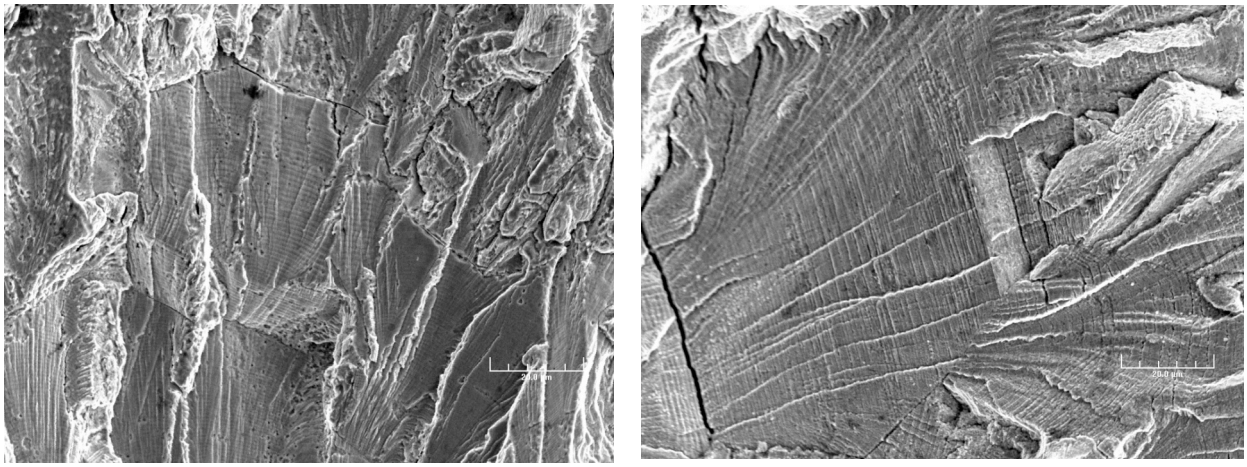

(c) (d)

Simulated PWR Environment

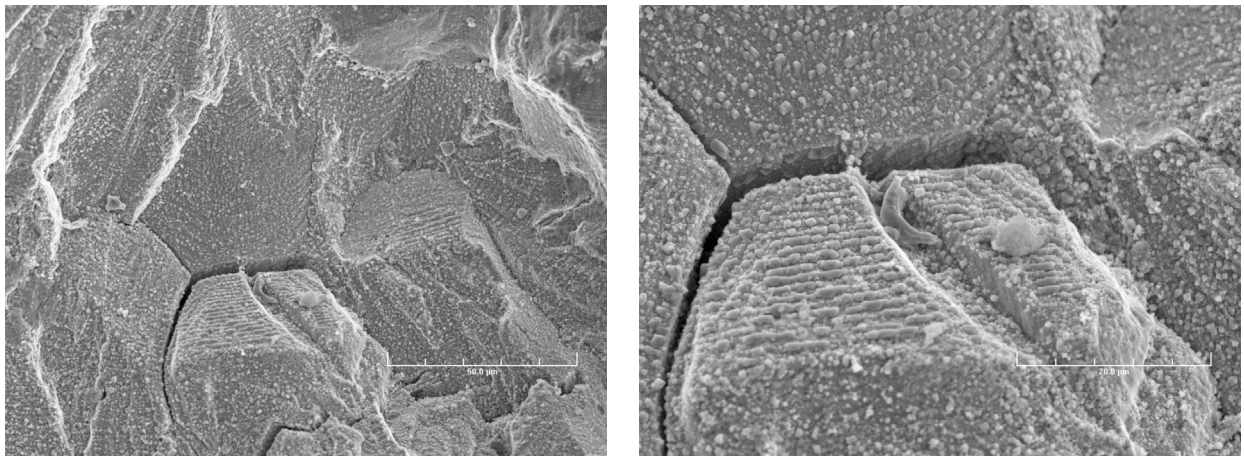

(e) (f)

Figure 12. Low– (a), (c), (e) and high–magnification (b), (d), (f) photomicrographs showing striations at select locations on fracture surfaces of MA specimens of Heat 10285 heat–treated for 24 h at 600°C in air, BWR, and PWR environments.

Heat 30956 mill annealed plus 24 h at 700°C

Air Environment

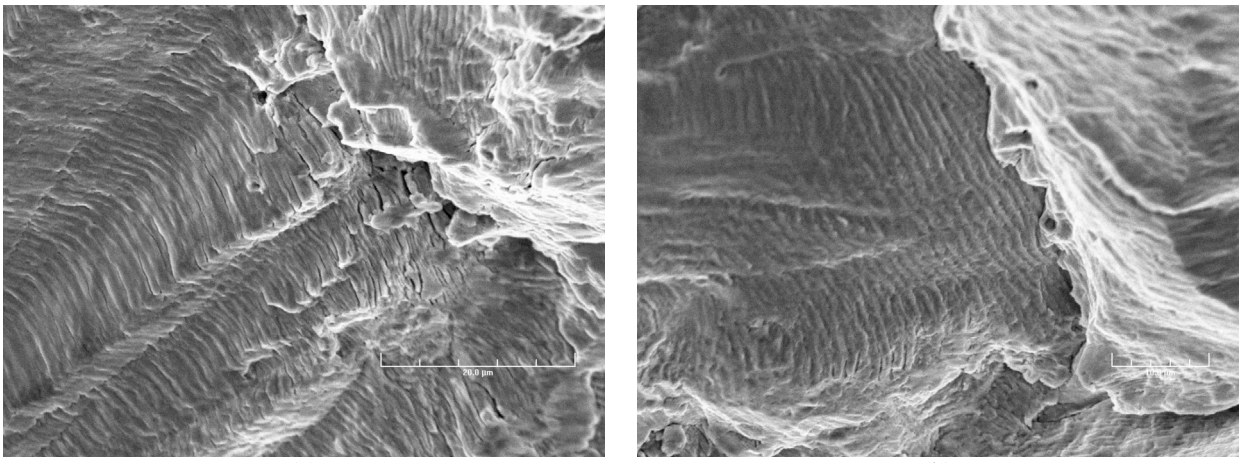

(a) (b)

Simulated BWR Environment

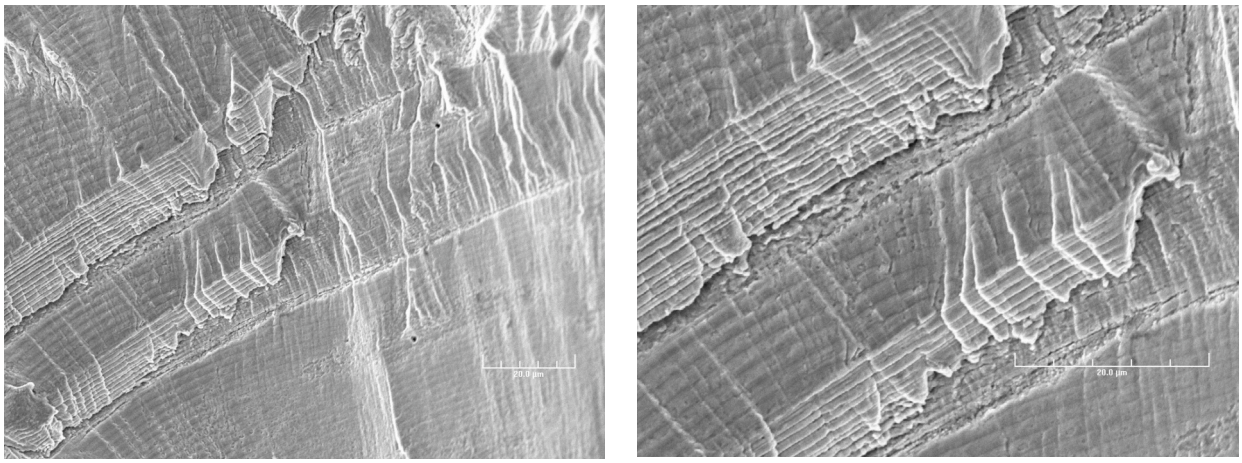

(c) (d)

Simulated PWR Environment

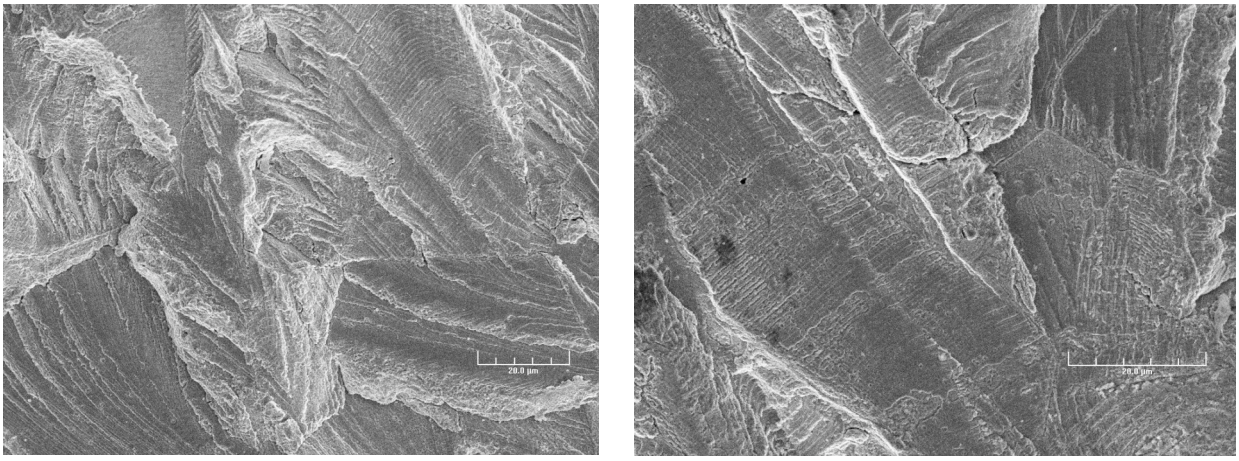

(e) (f)

Figure 13. Low– (a), (c), (e) and high–magnification (b), (d), (f) photomicrographs showing striations at select locations on fracture surfaces of MA specimens of Heat 30956 heat–treated for 24 h at 700°C in air, BWR, and PWR environments.

Photomicrographs of the crack morphology of Type 304 SS under all test and environmental conditions are presented in Fig. 14. In all cases, the tensile axis is vertical, parallel to the plane of each picture. In general, for air tests the cracks are more likely to be oblique, approaching 45° with respect to the tensile axis. By contrast, the cracks that form in either BWR or PWR environments tended to be perpendicular to the tensile axis.

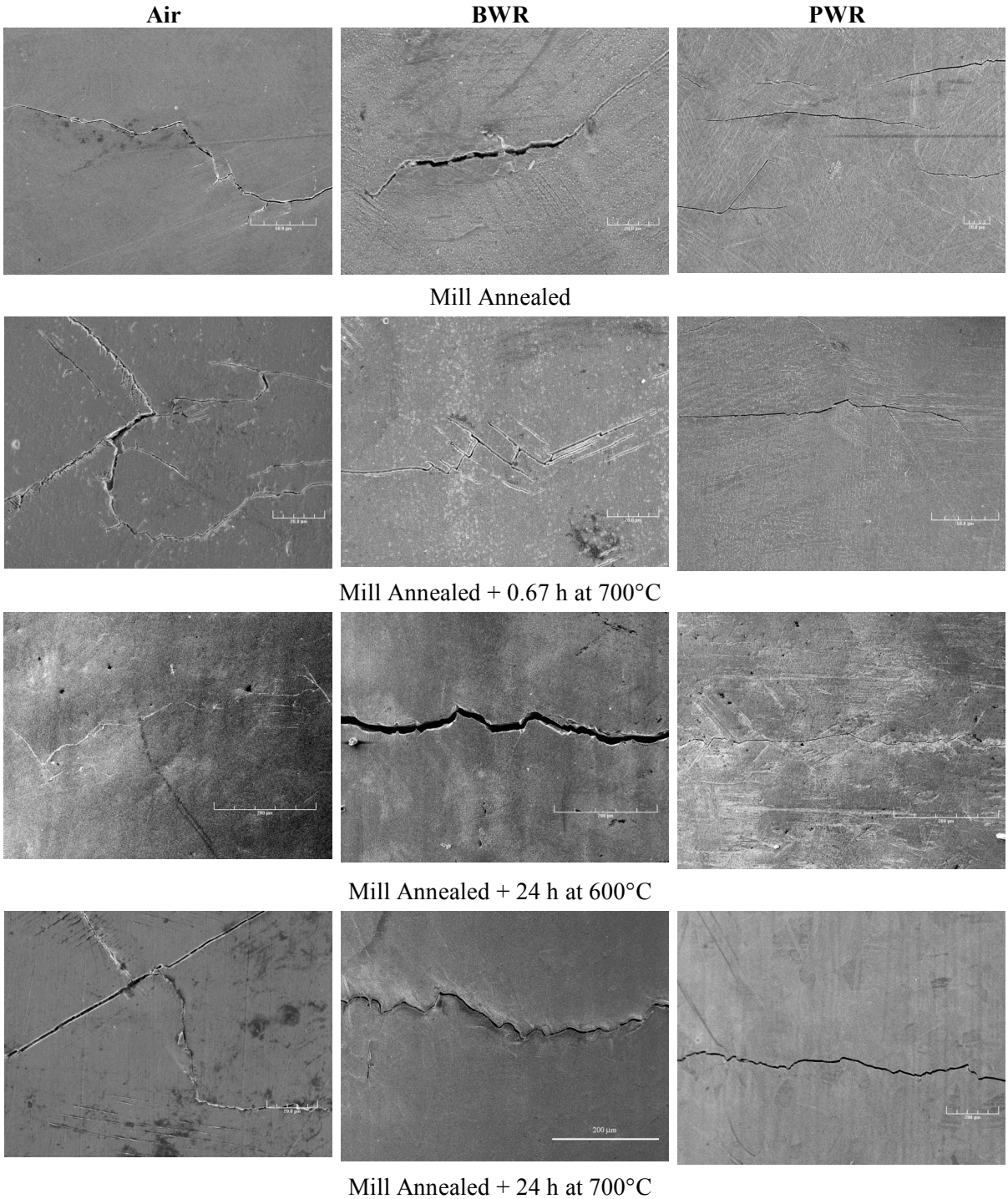

Figure 14. Photomicrographs of the crack morphology of Type 304 SS under all test and environmental conditions.

The results of the metallographic evaluations of the fatigue test specimens may be summarized as follows. In air, cracking was initiated as TG, oblique with respect to the tensile axis. In BWR environments, cracking was initiated as IG, normal to the tensile axis. By contrast, in PWR environments cracking was initiated as TG, but still normal to the tensile axis. Cracking propagated as TG irrespective of the environment.

The crack and fracture morphology in Type 316NG SS specimens (Heat D432804) from earlier tests was also evaluated for comparison. Figure 15 shows, at low and high magnification, crack initiation sites on the fracture surfaces of Type 316NG specimens tested in air. Note that the cracks were initiated and propagated in TG mode, most likely along crystallographic planes, leaving behind highly angular, cleavage–like or stepped surface features. Figures 15c and d show striations on some highly angular facets.

In a high–DO BWR environment, Fig. 16a–c, cracking was also initiated and propagated in TG mode, with riverlike patterns on the facets. Within 200 μm of the initiation site, fatigue striations were observed on some facets (Figs. 16b and c). Similarly, for specimens tested in a low–DO PWR environment (Fig. 16d), crack initiation and crack propagation are TG, with cleavage–like fracture facets

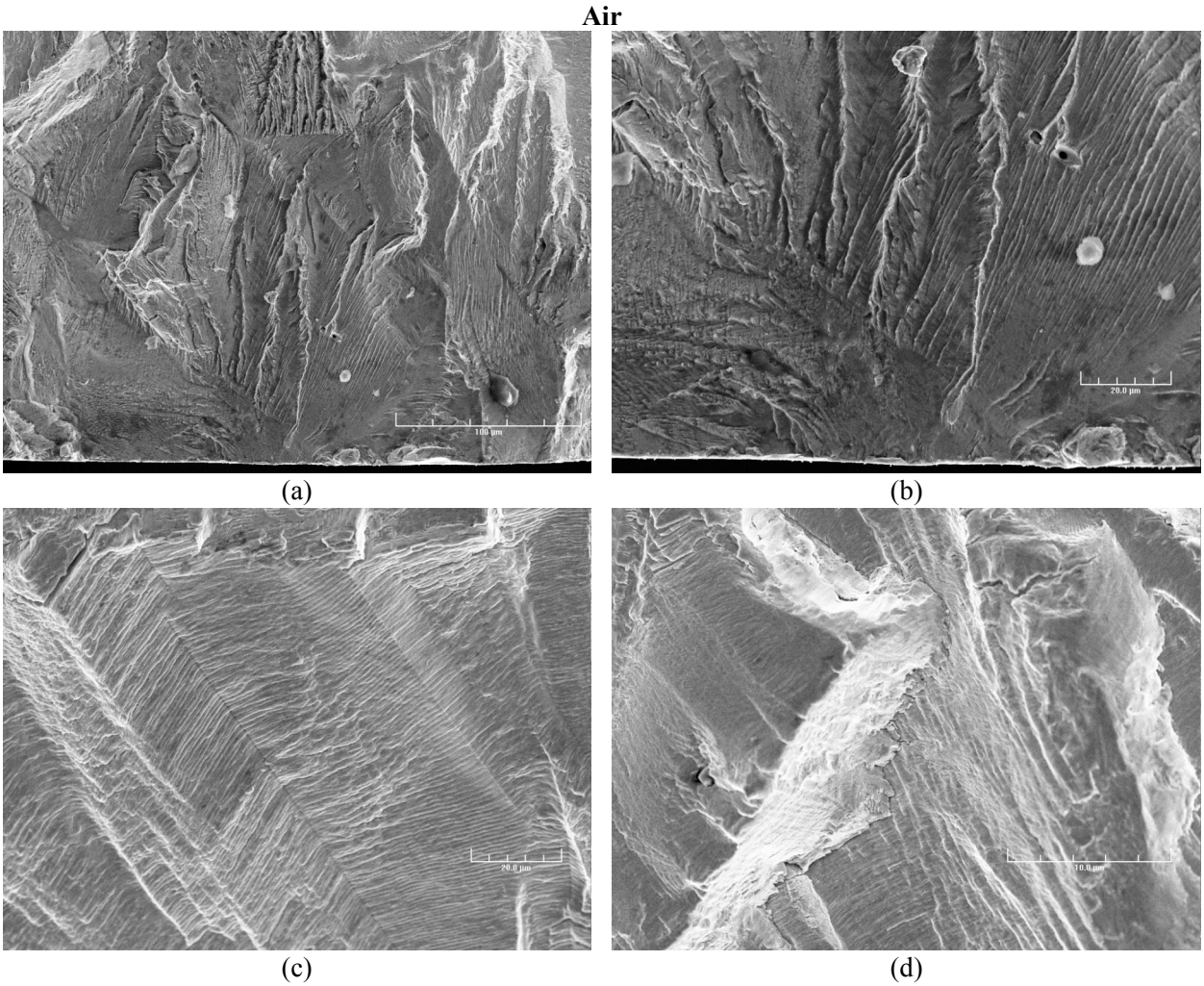

Figure 15. Photomicrographs showing crack initiation site at (a) low and (b) high magnification, and (c) and (d) striations at select locations in Type 316NG SS tested in air.

that exhibit river patterns. The higher magnification photomicrographs (at a location also seen in Fig. 16d) show fatigue striations within 200 μm of the initiation site. Evidence of rubbing due to repeated contact between the two mating surfaces can also be observed in Fig. 16f.

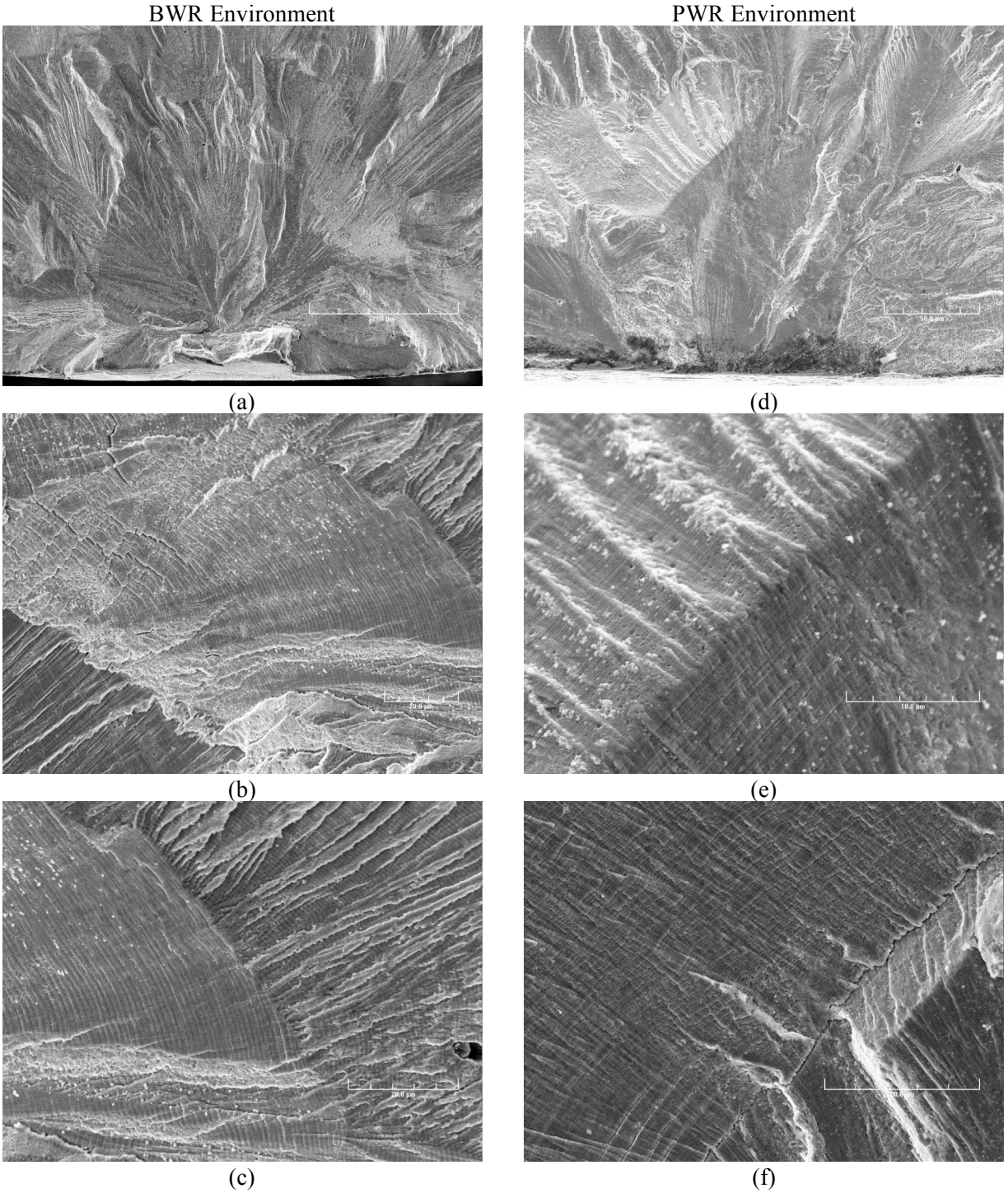

Figure 16. Photomicrographs showing crack initiation site and striations at select locations in Type 316NG SS tested in (a–c) BWR and (d–f) PWR environment.

Figure 17 presents photomicrographs that show the crack morphology in Type 316NG SS in three environments. In all cases, the tensile axis is vertical, parallel to the plane of each picture. The general appearance is that, for air tests, the cracks are more likely to be oblique, approaching 45° with respect to the tensile axis. By contrast, the cracks that formed in BWR environment appeared mixed, both oblique and normal to the tensile direction, while the cracks that formed in a PWR environment appeared mostly perpendicular to the tensile axis.

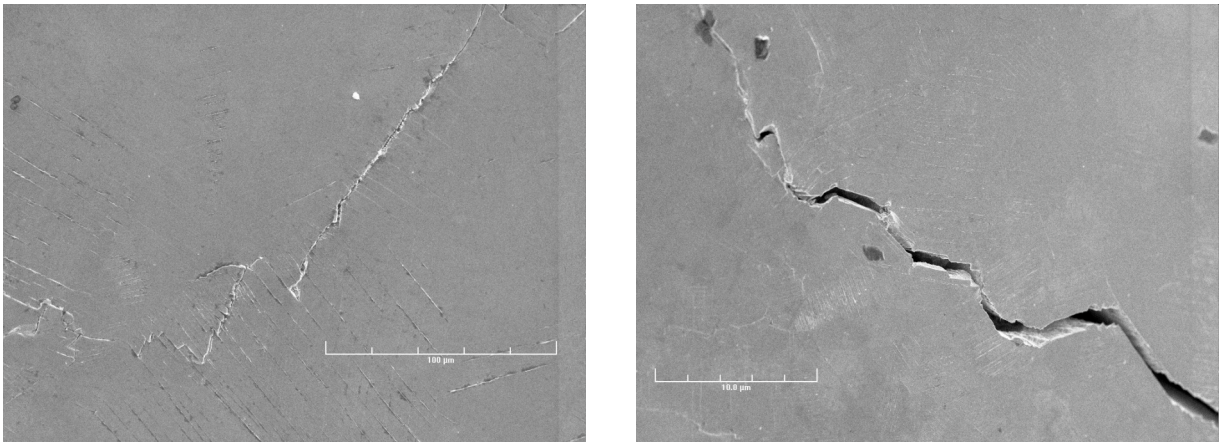

Air

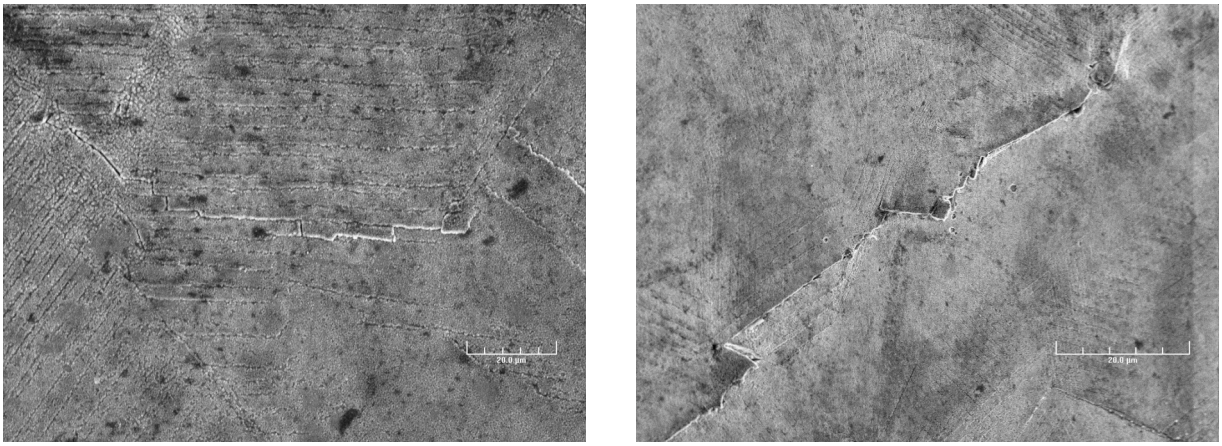

BWR Environment

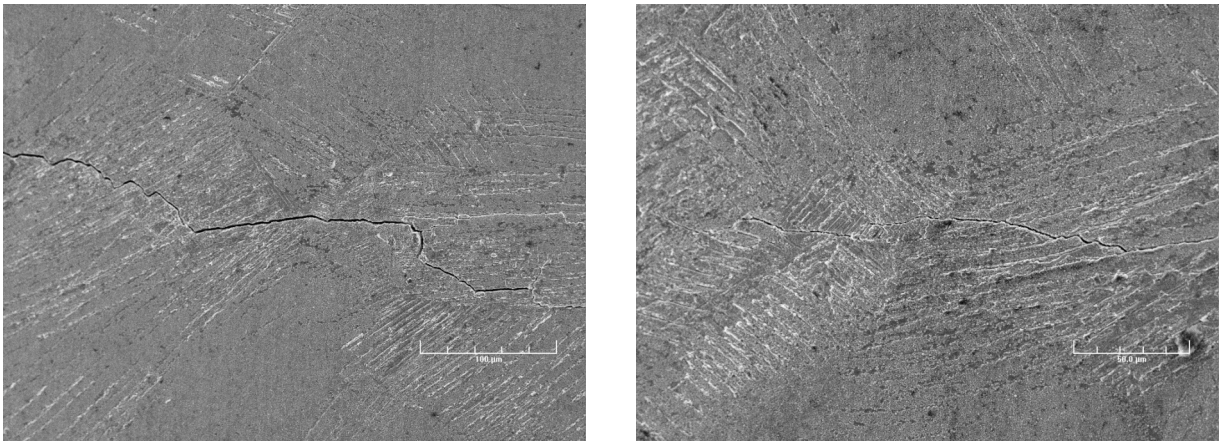

PWR Environment

Figure 17. Photomicrographs showing the morphology of lateral cracks formed in Type 316NG SS in three test environments.